Applied Energy 183 (2016) 61–76

Contents lists available at ScienceDirect

Applied Energy

journal homepage: www.elsevier.com/locate/apenergy

Electric power generation via plate type power generation unit from solar pond using thermoelectric cells

L.C. Ding *, A. Akbarzadeh, Abhijit Date

Energy Conservation and Renewable Energy, School of Aerospace Mechanical and Manufacturing Engineering, RMIT University, Bundoora East Campus, Australia

HIGHLIGHTS

- The design of a plate type power generation unit coupling with solar pond using TECs is proposed.
- An open channel power generation unit operates at atmospheric pressure is realised.
- The power generation unit is able to generate favourable power even at low flow rate.

ARTICLE INFO

Article history:
Received 25 May 2016
Received in revised form 26 August 2016
Accepted 27 August 2016

Keywords:
Solar pond
Heat exchanger
Thermoelectric
Power generation
Energy conversion

ABSTRACT

Solar pond (SP) has been a reliable supply of heat source for heating process that requires temperature <100 °C. In this work, the capability of solar pond in generating electricity has been explored experimentally using a plate type power generation unit (PTPGU). The open channel PTPGU was designed and fabricated in order to accommodate the TECs. The heat stored in the lower convective zone (LCZ) is used as the heat source needed for generating electricity by utilising thermoelectric cells (TECs) and thus a combined SP-PTPGU system is proposed. The PTPGU was tested with different hot water temperatures and flow rates. Also, the possibility of performance enhancement utilising copper mesh as insertion is presented. From the testing conducted, the PTPGU is able to generate 35.9 W of electricity at the flow rate as low as 5.1 LPM (litre per minute) at the hot water temperature of 81 °C. Besides coupling with solar pond, the PTPGU designed can also be coupled with other type of hot water source, such as hot spring.

1. Introduction

As advocated by Rowe [1] and Bell [2], thermoelectric cell is a solid state heat engine will be able to perform a vital role in providing an alternative solution for sustainable power generation as long as its current limitation of low conversion efficiency and high cost per watt is overcome in the future. To date, the commonly available thermoelectric generators (TEGs) which are made of bulk material Bi_2Te_3, come with a ZT value of around 1 [3]. The summaries of the recent advancement on the development of thermoelectric applications for power generation are available from the review conducted by Zheng et al. [4] and He et al. [5]. In order to produce electrical energy from thermoelectric cells, heat is supplied at the hot junction and is removed at the cold junction in order to create a temperature difference across the junction. Typically, either water or air is used as the heat transfer medium of the heat sink. In the study presented by Yu and Zhao [6], the TEG system under a parallel plate heat exchanger arrangement was studied in one dimensional analysis. From the analysis, a linear variation of temperature profile across the length of the heat exchanger for both parallel flow and counter flow type of setting, which is different from conventional logarithmic variation of temperature profile in parallel plate heat exchangers. The numerical model presented has been compared with the experimental result in a later publication [7]. Using electric power maximizing configuration with ΔT of 120 °C, 56 pieces commercially available Bi_2Te_3 TEGs will able to produce 147 W of electric power with a conversion efficiency of 4.4%. Meanwhile, for water cooled heat exchanger with TEGs, David et al. [8] delineated an optimisation method for maximizing the power output via heat exchanger optimisation for thermoelectric heat pump for geothermal applications. In the design, the hot side and cold side flow channel was able to work interchangeably, depending on the operating mode of the heat pump. They showed, there is an optimal thermal point that leads to the maximum coefficient of performance of the heat pump for a given fluid temperature. Moreover, a computational study has been conducted by other researcher by taking into account the dependency of thermoelectric properties on temperature.

* Corresponding author.
E-mail address: lcding@hotmail.com (L.C. Ding).

http://dx.doi.org/10.1016/j.apenergy.2016.08.161
0306-2619/

Nomenclature

Abbreviations

LCZ	lower convective zone
LMTD	log mean temperature difference
LPM	litre per minute
NCZ	non-convective zone
PTPGU	plate type power generation unit
SP	solar pond
TEG	thermoelectric generator
UCZ	upper convective zone

Symbols

b	height (mm)
c_p	specific heat (J/kg °C)
D_h	hydraulic diameter (m)
ΔP	pressure drop (Pa)
ΔT	temperature difference (°C)
f	friction factor
h	convection heat transfer coefficient (W/m^2 °C)
I	current (A)
k	thermal conductivity (W/mK)
l	length (m)
n_p	number of plates
$\dot{P}$	pumping power (W)
$\dot{Q}$	rate of heat transfer (W)
R	thermal resistance (W/°C)
r	electrical resistance (Ω)
S	salinity (g/kg)
T	temperature (°C)
V	voltage (V)
$\dot{V}$	flow rate (m^3/s)
w	gap size (mm)
$\dot{W}$	electric power (W)
α	mixing coefficient
β	mixing coefficient
ε	absolute surface roughness (mm)
η	efficiency
ρ	density (kg/m^3)
μ	dynamic viscosity (Pa S)
ω	error

Subscripts

c	cold
e	electric
g	glue
i	row number
in	inlet
j	column number
oc	open circuit
out	outlet
p	plate
s	steel
sc	short circuit
sg	steel and glue
T	total
w	water

Rodriguez et al. [9] described a one dimensional computational model that will aid the designer to simulate the performance of the TEG, by considering the variation of room temperature, electric load resistance as well as heat flux.

On the other hand, for air cooled TEG systems, Crane and Jackson [10] performed an investigation on optimising the TEG heat exchanger using a cross flow configuration. After taking into account the pumping requirements, their analysis showed that heat exchangers with Bi_2Te_3 TEGs will be able to achieve net power per unit volume of 45 kW/m^3 for a heat exchanger sized at producing 1 kW$_e$. On the other hand, Suter et al. [11] performed geometrical optimisation for a 1 kW$_e$ thermoelectric stack using a geothermal heat source. With similar type of configuration, Gou et al. [12] suggested several improvements that can be done on enhancing the system performance, such as taking into consideration the parallel/series connection of the TEGs as well as taking appropriate measures to increase the heat transfer at the heat sink by extending its surface area. To further elaborate the point of improving the heat transfer for the TEG-heat exchanger system, Nnanna et al. [13] proposed the use of nanofluids such as Al_2O_3-H_2O, which has the potential on reducing the contact resistance of the TEG and heat exchanger and thus enhancing the heat transfer.

Research has also been conducted on converting the heat available from automobile exhaust [14–16]. Furthermore, in order to enhance the heat transfer of the heat exchanger for harvesting the exhaust heat into electricity, different methods could be applied such as the use of a dimpled surface to replace the need of using fin proposed by Wang et al. [17], applying metal foam inserts into the heat exchanger [18] and minimising the contact thermal resistance in the heat exchanger [19]. Hsu et al. [20] developed a system consisting of 24 pieces of Bi_2Te_3 TEGs. From their study, they emphasized that a proper thermal distribution will improve both the thermal and electric performance. Despite the fact that a low heat input will eventually lead to low conversion efficiency, they opined, it will not be a major concern since the heat source is freely available. If a free heat source is available, such as from a hot spring, the research work conducted by Sasaki et al. [21] has shown that a TEG system incorporated with the hot spring is able to generate 1.927 MW h in 8966 h of operation. Recent study on the thermoelectric heat recovery system by using water as working fluid at hot side temperature <80 °C in both transient and steady state condition had been carried out by Massaguer et al. [22] along with a verified thermoelectric energy harvesting model through experiment. For coolant based working fluid, Bjørk et al. [23] realised a thermoelectric power generation system based on 100 pieces commercially available thermoelectric generators at the flow rate as low as 5.0 LPM. With a fluid temperature difference of 175 °C, their system generated 200 W of electric power.

As a large scale solar energy collector and energy storage system, the solar pond (SP) collects the solar radiation transmitted into the SP and stores the heat in the lower convective zone (LCZ) with saturated salt (usually NaCl) solution. The non-convective zone (NCZ) minimises the heat loss by suppressing the convection heat loss to the top of the SP. Working as both thermal collector and thermal storage, solar ponds absorb the energy radiated from the sun and as a result, the radiation energy that penetrates to the lower convective zone is stored, owing to the density variation of the solar pond. The heat stored in the SP is in the regime of low grade heat and ranges up to the boiling point of saturated salt solution at atmospheric condition. As an illustration of the characteristics of the SP, Fig. 1 represents a typical temperature and density profile of a 50 m^2, 2.05 m depth research solar pond available in RMIT, Melbourne, whereas Fig. 2 shows the temperature profile of an operating commercial solar pond at Granada, Spain. Research from the past decades has shown successful application of solar ponds in providing the heat needed for heating applications or generating electricity by using organic Rankine cycle [24].

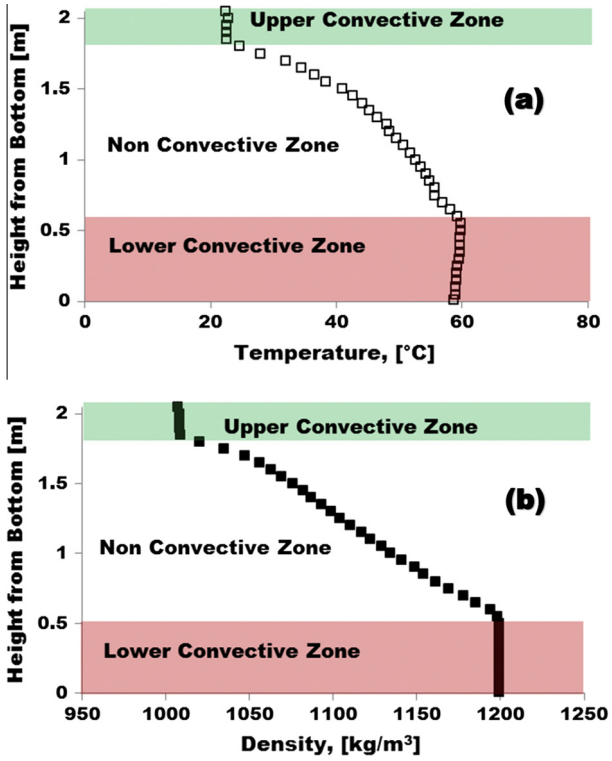

Fig. 1. The typical temperature (a) and density (b) profile for RMIT solar pond.

This study presents the design of a plate type power generation unit (PTPGU) using commercially available Bi_2Te_3 TECs that are being accommodated in a parallel plate counter flow heat exchanger. The application of PTPGU is targeted on coupling the unit with the solar pond (which will provide the heat source needed for PTPGU) as given in Fig. 3. In contrast to the use of organic Rankine cycle for the power generation from SP, the PTPGU presented in this study provides a simplest design for power generation that involves no moving part. Moreover, the TECs for power generation with heat exchangers presented to date are usually in the closed loop condition. Thus, higher pumping power is needed in order to compensate the pressure drop. Instead of adopting a closed loop design, the PTPGU introduced in this paper explores the potential of an open channel design that operates at atmospheric pressure, which demarcates from the conventional design.

2. The design issues of PTPGU

In the early stages of the heat exchanger design, the consideration is required in terms of the selection of the flow arrangement, surface material as well as size and shape. In order to cater to the shape of commercially available thermoelectric generators, a heat exchanger with a flat surface is preferred. From the review conducted, there is no research conducted on open channel plate type heat exchanger incorporating TEC for power generation. In order to attach the TECs to the plates, thermal adhesive is used. Prior work conducted by Singh et al. [25] justified the used of the thermal adhesive that will able to provide the lowest thermal resistance.

Besides the uncertainty in the basic design correlation for the design of a water to water heat exchanger, it is crucial that there is no mixing of both hot and cold streams. The maldistribution of flow in the heat exchanger happens when the flow is not uniformly distributed along the core of heat exchanger. In light of the flow maldistribution, the thermal performance of the heat exchanger will be significantly lower than predicted and the pressure drop across the heat exchanger is elevated at the same time. If the working fluid and heat exchanger surface is sensitive to erosion, the region with higher flow rate will be susceptible to further wear. In order to address the issues above, a PTPGU with an open channel flow design is attempted. Instead of designing a PTPGU with closed channel flow, the open channel PTPGU is operating at atmospheric pressure and there will be minimal cross-plate mixing. Furthermore, in terms of accessibility, since commercially available TECs are embedded in the PTPGU without a fully enclosed housing, such design offers the ease in the maintenance of PTPGU. Fig. 4(a) shows the effect of the outlet position on the overall flow distribution in a channel at a flow rate of 0.1 L/s in a channel with 4 mm gap. Generally, the bottom outlets will have a higher flow rate compared to the upper outlets due to the difference of head. Visually, the branching design of A, B and E will provide satisfactory flow distribution and minimal stagnant region. Furthermore, in order to better distribute the water on to the channels, the passage of the inlet is tapered to maintain a constant pressure drop across the delivery line. Fig. 4(b) illustrates the design of the inlet and outlet of the PTPGU in this study.

3. Theoretical modelling

3.1. Heat transfer modelling

The heat transfer model in this section is established on the basis of there is minimal flow maldistribution in the heat

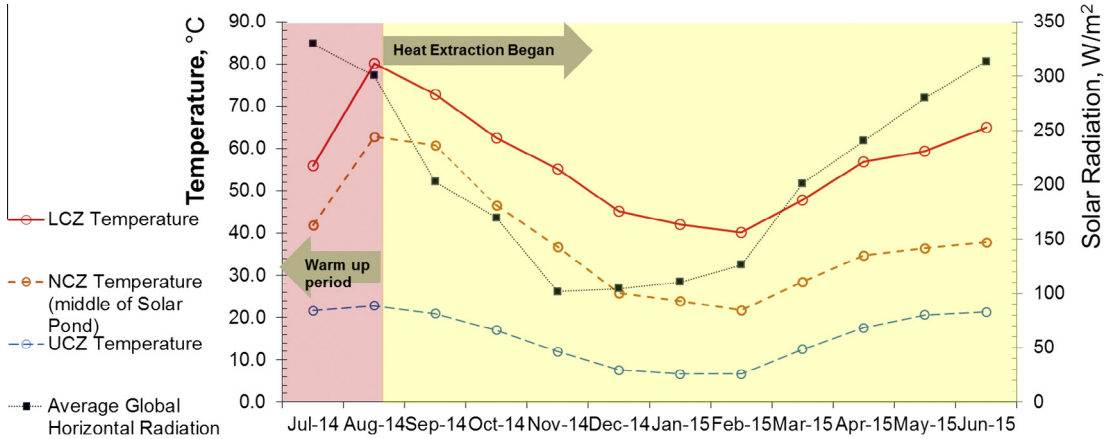

Fig. 2. The monthly temperature profile of an operating commercial solar pond at Granada, Spain.

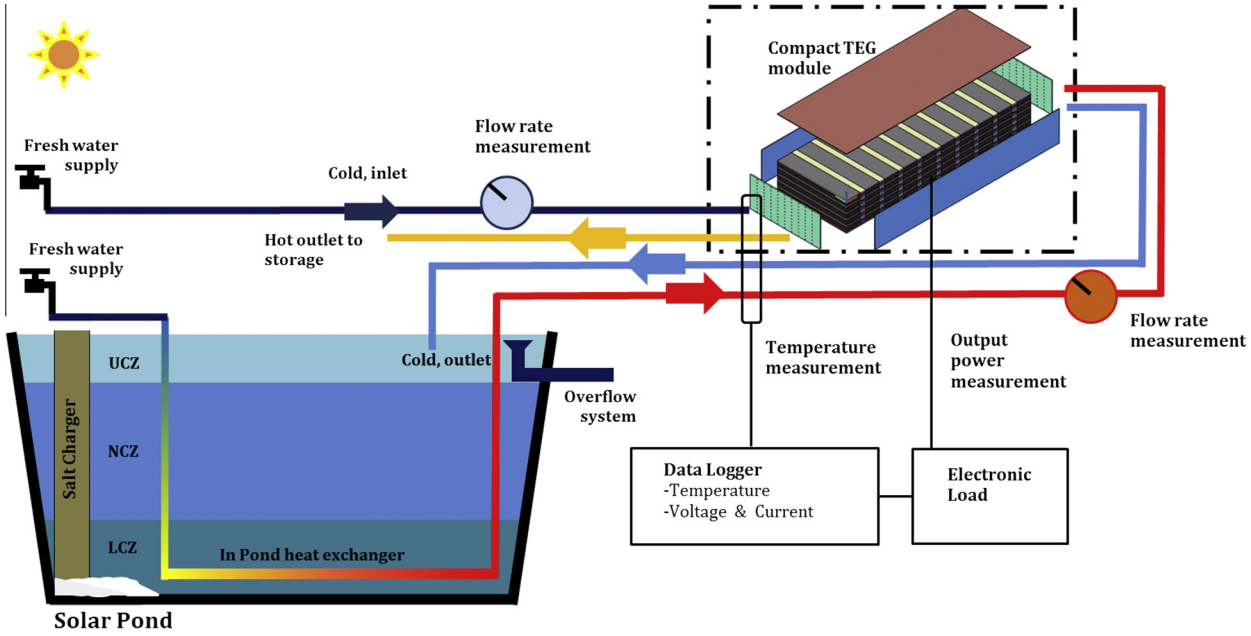

Fig. 3. The proposed SP-PTPGU system.

exchanger and also there is minimal heat loss to the surrounding which can be ignored. The thermal properties of the fluid in the model are estimated by using the equations listed in Table 1.

The estimation of the Nusselt number of turbulent flow is performed by using the correlation given by

$$Nu = 0.023Re^{0.8}Pr^{n} \tag{1}$$

where $n = 0.4$ for heating process and $n = 0.3$ for cooling, whereas for laminar flow condition, $Nu = 8.235$. The Reynolds number across the parallel plates with gap w_c and w_h for cold side and hot side, respectively, are

$$Re_c = \frac{\rho_{wc,in}\dot{V}D_{h,c}}{bw_c\mu_{wc,in}} = \frac{\rho_{wc,in}\dot{V}_cD_{h,c}}{(\frac{n_p}{2}+1)bw_c\mu_{wc,in}} = \frac{2\rho_{wc,in}\dot{V}_cb}{(\frac{n_p}{2}+1)(w+b)jl_t\mu_{wc,in}} \tag{2}$$

$$Re_h = \frac{\rho_{wc,in}\dot{V}D_{h,h}}{bw_h\mu_{wc,in}} = \frac{\rho_{wc,in}\dot{V}_hD_{h,h}}{bw_h\mu_{wc,in}} = \frac{4\rho_{wh,in}\dot{V}_hb}{n_p(w+b)jl_t\mu_{wc,in}} \tag{3}$$

The Prandtl number and the dynamic viscosity of the fluid is estimated by using the relation listed by Sharqawy et al. [27] and subsequently the convection heat transfer coefficient, h is estimated through $h = \frac{Nu\times k}{D_h}$.

3.1.1. The discrete element method

In this subsection, the heat transfer for the PTPGU is modelled using the discrete element method. Fig. 5 shows the notation of each TEC located at the same plate. In the design of the PTPGU, there will be n_P number of plates arranged parallelly to the direction of the flow. The TECs aligned in the direction parallel to the flow is denoted as column- j^{th} whereas for the TECs arranged in the direction perpendicular to the flow is noted as row- i^{th}. In this model, the TECs at the same j^{th} column is modelled as single entity and the heat transfer is assumed flowing through the cells since the gap between each cell is insulated and the heat transfer across the insulating material is insignificant. Fig. 6 delineates the example of the heat transfer calculation for the selected cells in the PTPGU by adopting discrete element method. In the model, the working fluid aligned at the same j^{th} column will have the same temperature since it is located at the same cross sectional plane perpendicular to the direction of flow. The calculation of the heat transfer across each TEC requires the knowledge of the thermal resistance through its thermal resistance network and Fig. 7 presents the complete thermal resistance network for the PTPGU. The thermal resistances as shown in Fig 7, consist of the resistant caused by convective heat transfer (for both hot and cold side of the flow), the conduction heat transfer resistant by the TECs, adhesive as well as the plates.

The solution for the equations in the table above requires the equations to be solved simultaneously for $j(n+1)-n$ unknowns.

For Plate-1 and Plate-n, the resistance network is

$$R'_T = \mathrm{j}\sum R_{wc,ij} + \sum R_{TEC,ij} + \sum R_{g,ij} + \sum R_{s,ij} + \frac{\mathrm{j}\sum R_{wh,ij}}{2} \tag{4}$$

Whereas for Plate $\neq$1or$\neq$n, the resistance network is

$$R_T = \frac{\mathrm{j}\sum R_{wc,ij}}{2} + \sum R_{TEC,ij} + \sum R_{g,ij} + \sum R_{s,ij} + \frac{\mathrm{j}\sum R_{wh,ij}}{2} \tag{5}$$

Alternatively, to put in a simpler form, $R_{T'} = R_T + \frac{\mathrm{j}\sum R_{wc,ij}}{2}$

3.1.2. The lump capacitance method

Instead of using the discrete element method described in the previous subsection, the heat transfer in the PTPGU can be estimated by using the lump capacitance method. From the numerical comparison conducted, there is insignificant difference in the estimated output which is less than 2%.

For the hot streams,

$$\dot{Q}_h = -\dot{m}_hc_{p,h}(T_{h,in} - T_{h,out}) \tag{6}$$

Whereas for cold streams,

$$\dot{Q}_c = \dot{m}_cc_{p,c}(T_{c,in} - T_{c,out}) \tag{7}$$

Assuming ideal condition with no losses to the ambient, it requires that

$$\dot{Q}_h + \dot{Q}_h = 0 \tag{8}$$

$T_{c,out}$ and $T_{h,out}$ are the unknown that need to be solved. Hence log mean temperature difference (LMTD) method for heat exchanger is needed to provide second equation for solving two unknowns. LMTD is defined as, $\Delta T_{lmtd} = \frac{\Delta T_1 - \Delta T_2}{\ln\left(\frac{\Delta T_1}{\Delta T_2}\right)}$ where $\Delta T_1 = T_{h,in} - T_{c,out}$ and $\Delta T_2 = T_{h,out} - T_{c,in}$.

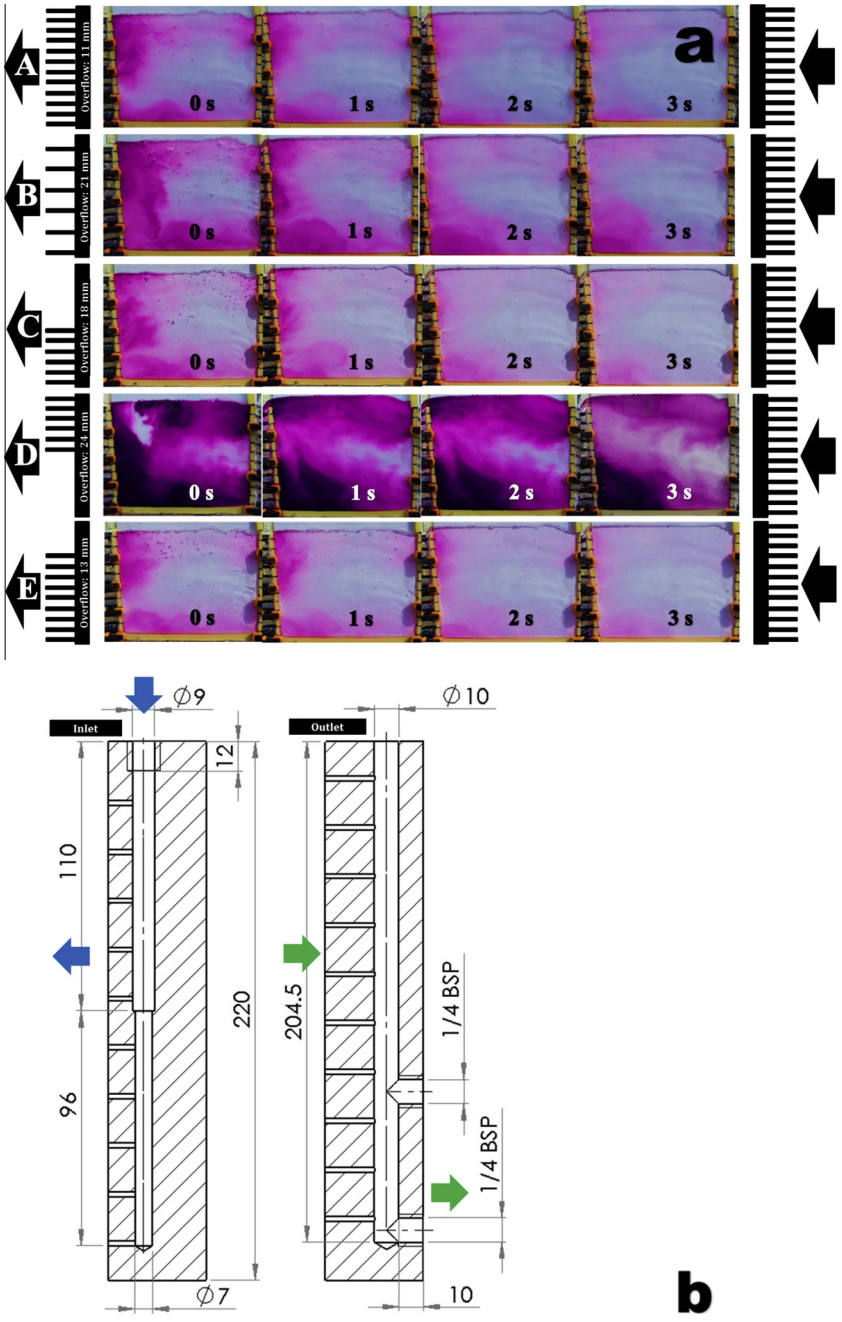

Fig. 4. Flow visualisation of the effect of outlets on flow distribution (a) and (b) the design of the inlet and outlet of the PTPGU (dimension in mm).

The amount of heat transferred is then

$$q = UA\Delta T_{lmtd} \tag{9}$$

Table 1
Thermal properties estimation of working fluid [26].

Thermal Properties	Equations
Density (kg/m^3)	$\rho_w = 998 + 0.65S - 0.4(T - 20)$ T and S represent the fluid temperature (°C) and salinity (in g/kg), respectively
Specific heat (J/kg °C)	$c_p = 4180 - 4.396S + 0.0048S^2$ where S represent the fluid salinity (in g/kg)
Thermal conductivity (W/m °C)	$k_w = 0.5553 - 0.0000813S + 0.0008(T - 20)$, T and S represent the fluid temperature (°C) and salinity (in g/kg), respectively

where

$$\begin{aligned}\frac{1}{UA} &= \frac{1}{U_cA_c} = \frac{1}{U_hA_h} \\ &= \frac{1}{(hA_p)_c} + \left(\frac{1}{\frac{d_{TEC}}{k_{TEC}A_{TEC}} + \frac{d_{glue}}{k_{glue}A_{glue}}} + \frac{1}{\frac{d_{TEC}+d_{glue}}{k_{filler}A_{filler}}}\right)^{-1} + \frac{d_P}{k_pA_p} + \frac{1}{(hA_p)_h} \\ &= \frac{1}{(hA_p)_c} + \left(\frac{ij}{R_{TEG} + R_{glue}} + \frac{1}{\frac{d_{TEC}+d_{glue}}{k_{filler}A_{filler}}}\right)^{-1} + \frac{d_P}{k_pA_p} + \frac{1}{(hA_p)_h}\end{aligned} \tag{10}$$

and $A_c = A_h = A_p = A_{TEC} + A_{filler} = A_{glue} + A_{filler}$. The total heat transfer of the system is evaluated by multiplying Eq. (9) with n_p,

$$\dot{Q} = n_pUA\Delta T_{lmtd} \tag{11}$$

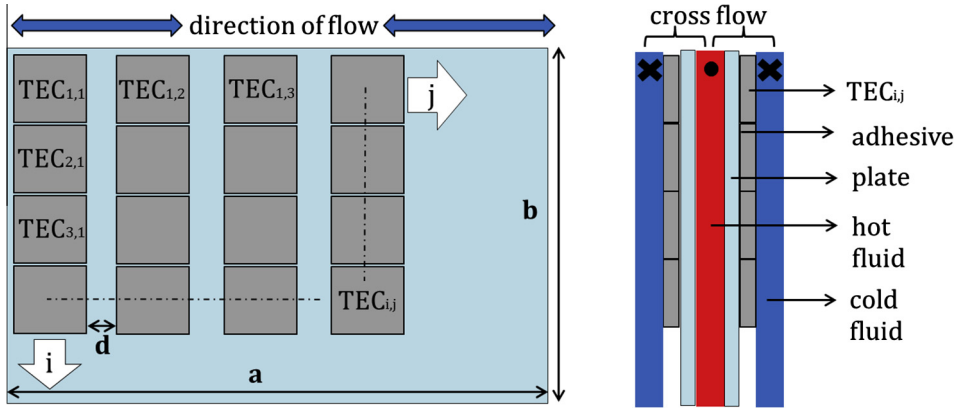

Fig. 5. The notation for theoretical model and its cross sectional view.

j	Plate 1	Plate 1 Plate 2	Plate 2 Plate 3	Plate 3 Plate 4	.....	Plate n
	Cold Inlet	Hot Outlet	Cold Inlet	Hot Outlet	.....	Cold Inlet
1	$T_{wc@C1,1}$	$T_{wh@H1,1} = T_{wh@H1,2} + \frac{T_{wc@C1,2} - T_{wh@H1,2}}{\dot{m}c_{ph}R'_T} + \frac{T_{wc@C2,2} - T_{wh@H1,2}}{\dot{m}c_{ph}R_T}$	$T_{wc@C2,1}$	$T_{wh@H2,1} = T_{wh@H2,2} + \frac{T_{wc@C2,2} - T_{wh@H2,2}}{\dot{m}c_{ph}R_T} + \frac{T_{wc@C3,2} - T_{wh@H2,2}}{\dot{m}c_{ph}R_T}$		$T_{wc@Cn+1,1}$
2	$T_{wc@C1,2} = T_{wc@C1,1} + \frac{T_{wh@H1,1} - T_{wc@C1,1}}{\dot{m}c_{pc}R'_T}$	$T_{wh@H1,2} = T_{wh@H1,3} + \frac{T_{wc@C1,3} - T_{wh@H1,3}}{\dot{m}c_{ph}R'_T} + \frac{T_{wc@C2,3} - T_{wh@H1,3}}{\dot{m}c_{ph}R_T}$	$T_{wc@C2,2} = T_{wc@C2,1} + \frac{(T_{wh@H1,1} - T_{wc@C2,1})}{\dot{m}c_{pc}R_T} + \frac{(T_{wh@H2,1} - T_{wc@C2,1})}{\dot{m}c_{pc}R_T}$	$T_{wh@H2,2} = T_{wh@H2,3} + \frac{T_{wc@C2,3} - T_{wh@H2,3}}{\dot{m}c_{ph}R_T} + \frac{T_{wc@C3,3} - T_{wh@H2,3}}{\dot{m}c_{ph}R_T}$		$T_{wc@Cn+1,2} = T_{wc@Cn+1,1} + \frac{T_{wh@Hn,1} - T_{wc@Cn+1,1}}{\dot{m}c_{pc}R_T}$
⋮	⋮	⋮	⋮	⋮	⋮ ⋮	⋮
j	$T_{wc@C1,j} = T_{wc@C1,j-1} + \frac{T_{wh@H1,j-1} - T_{wc@C1,j-1}}{\dot{m}c_{pc}R'_{T'}}$	$T_{wh@H1,j}$	$T_{wc@C2,j} = T_{wc@C2,j-1} + \frac{(T_{wh@H1,j-1} - T_{wc@C2,j-1})}{\dot{m}c_{pc}R_T} + \frac{(T_{wh@H2,j-1} - T_{wc@C2,j-1})}{\dot{m}c_{pc}R_T}$	$T_{wh@H2,j}$		$T_{wc@Cn+1,j} = T_{wc@Cn+1,2} + \frac{T_{wh@Hn,j-1} - T_{wc@Cn+1,j-1}}{\dot{m}c_{pc}R_T}$
	Cold Outlet	Hot Inlet	Cold Outlet	Hot Inlet	.....	Cold Outlet

Note: The subscript notation is explained as follows:

- w: water
- h: hot side / c: cold side
- $@Cn$: Cold channel no. n , whereas $@Hn$: Hot channel no. n
- j: TEC row number

Fig. 6. The temperature distribution calculation of the PTPGU using discrete method.

The geometrical information and working fluid conditions involved in the parametric study are presented in Tables 2 and 3, respectively.

3.2. Estimation of pumping power

The modified Colebrook equation, given by Haaland with ±5% error with experimental data is used as to avoid the iteration procedure due to the implicit nature of friction factor, f in the original Colebrook equation. For turbulent flow,

$$\frac{1}{\sqrt{f}} = -1.8\log\left[\frac{6.9}{Re} + \left(\frac{\frac{\varepsilon}{D_h}}{3.7}\right)^{1.11}\right] \tag{12}$$

For the flow under laminar regime ($Re < 2300$), $f_c = \frac{96}{Re_c}$ and $f_h = \frac{96}{Re_h}$ for the friction factor of cold and hot side, respectively.

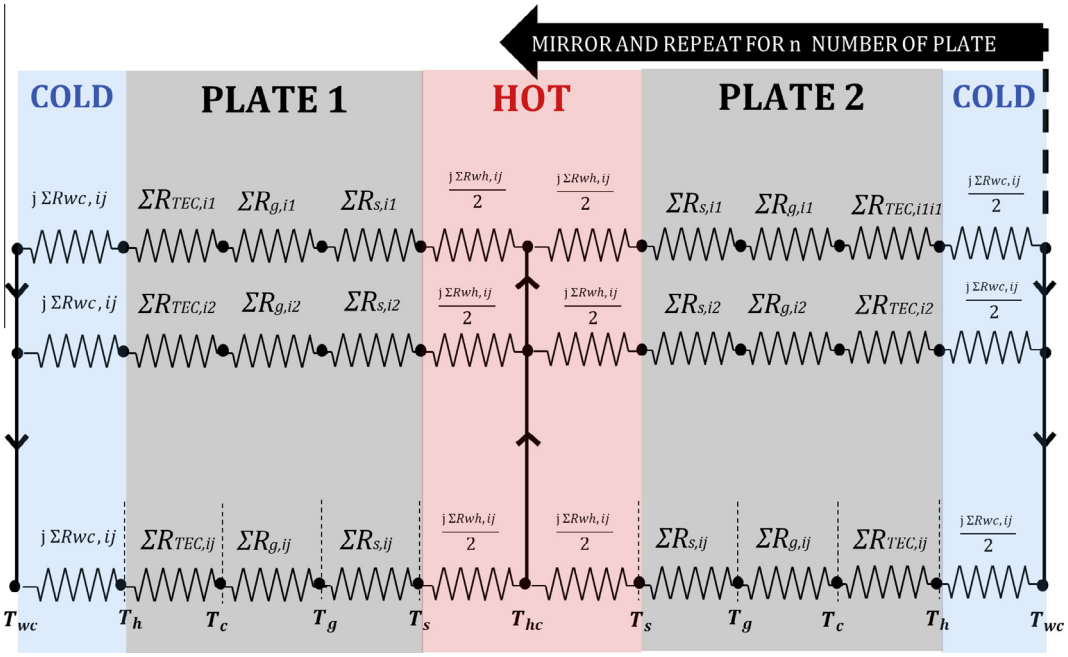

Fig. 7. The thermal resistance network of the PTPGU using discrete method.

Table 2
Geometrical parameters for theoretical study.

Items	Equations	Value (if any)
TEC dimensions	Side length, l_t Total TEC area, $A_{TEC} = ijl_t^2$	$l_t = 40$ mm
Plate dimensions (refer to Fig. 5) i. width, a ii. height, b iii. area, A_p	$a = jl_t + jd$ $b = il_t$ $\delta = d/l_t$ $A_p = ab = ijl_t^2(1+\delta)$	i and j are subjected to optimisation $\delta = 0.5$
Filler material i. Area, A_{filler}	$A_{filler} = A_p - A_{TEC} = \delta ijl_t^2$	Filler material (silicone) thermal conductivity, 0.1 W/m °C
Fluids passage i. Gap for cold side, w_c ii. Gap for hot side, w_h	Hydraulic diameter $D_{h,c} = \frac{2w_c il_t}{(w_c + il_t)}$ $D_{h,h} = \frac{2w_h il_t}{(w_h + il_t)}$	Value of w_c and w_h are subjected to optimisation, with the constrain $w_c = w_h$
Number of Plates *Plate thickness*	n_p d_p	Subject to optimisation, with the constrain $n_p \times i \times j = 500$ 0.7 mm, $R_p = \frac{d_p}{kA_p}$ $k_p = 16$ W/m °C $R_p = 0.00073$ W/°C
TEC thickness *Adhesive thickness*	d_{TEC} d_{glue}	3 mm, $R_{TEC} = 0.7$ W/°C 1 mm, $R_{glue} = 0.1$ W/°C

Table 3
Working fluid conditions for theoretical study.

Parameters	Cold side		Hot side	
	Symbol	Value	Symbol	Value
Inlet temperature (°C)	$T_{c,i}$	20	$T_{h,i}$	90
Outlet Temperature (°C)	$T_{c,o}$	Calculated by solving Eqs. (6) or (7) with (9).	$T_{h,o}$	Calculated by solving Eqs. (6) or (7) with (9).
Total flow rate (L/s)	$\dot{V}_c$	0.5–5.0 L/s	$\dot{V}_h$	0.5–5.0 L/s
Flow rate per plate (L/s)	$\frac{\dot{V}_c}{\frac{n_p}{2}+1}$	Configuration dependent since $n_p = 4$, 10 or 20.	$\frac{2\dot{V}_h}{n_p}$	Configuration dependent since $n_p = 4$, 10 or 20.
Salinity (g/kg)	S	Pure water: 0 Low salinity water: 30	S	Pure water: 0 Saturated salt water: 350

The absolute surface roughness of stainless steel, $\varepsilon = 0.015$ mm is used in the estimation of friction factor. Note that the absolute surface roughness for ceramic should be used for the flow directly exposed to the ceramic casing of TEC. However, in this part, the equal value of surface roughness for both stainless steel and ceramic surface is assumed. For the pumping losses,

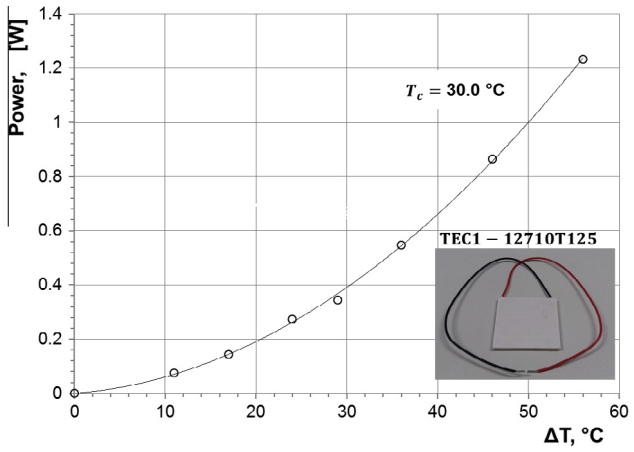

Fig. 8. The performance of single TEC for the output power estimation of PTPGU.

$$\Delta P_c = f_c \frac{a}{D_{c,h}} \frac{\rho_c}{2} \left(\frac{\dot{V}_c}{(\frac{n_p}{2}+1) b w_c} \right)^2 \quad (13a)$$

$$\Delta P_h = f_c \frac{a}{D_{h,h}} \frac{\rho_h}{2} \left(\frac{\dot{V}_h}{\frac{n_p}{2} b w_h} \right)^2 \quad (13b)$$

In turn, the pumping power is calculated by $\dot{P} = \Delta P \dot{V}$.

3.3. Estimation of electric power

In this study, commercially available TECs (TEC1-12710T125) were used as the thermoelectric power generation modules in the PTPGU. The performance of this TEC in generating electricity at a given temperature difference across the TEC was tested experimentally. In Fig. 8, the performance of electric power generated by single TEC is plotted against ΔT. The cold side temperature, T_c of the TEC was maintained at 30 °C. Note that a conservative value of $T_c = 30$ °C was used since although the cold inlet water inlet temperature of the PTPGU tested will range from 20 to 25 °C, due to the fact that the surface temperature of TEC will generally higher than the fluid temperature under convective heat transfer. The relation of $\dot{W}_{max}$ against ΔT established in Fig. 8 can be used to estimate the overall electric power generated by PTPGU since in Section 3.1, the ΔT across the TEC is readily known from heat transfer in the PTPGU established as $\Delta T_{TEC} = \dot{Q} R_{TEC}$ and $R_{TEC} = 0.7$ °C/W.

3.4. Optimising the design

In this subsection, the theoretical performance of PTPGU is presented. As the number of the TECs in the PTPGU is fixed at 500, 5

Table 4
Theoretical maximum net power performance of PTPGU.

Maximum Net Power Performance [a]	$i \times j \times$ Number of plate, n_p				
	$5 \times 5 \times 20$	$5 \times 10 \times 10$	$5 \times 25 \times 4$	$10 \times 5 \times 10$	$25 \times 5 \times 4$
Maximum Net Power (W)	446	432	398	443	431
Optimum Gap (mm)	2	3.5	5	2	2
Optimum Flow Rate (L/s)	5	5	3	5	5
Specific Power (W/m^3)	54.65	42.08	31.17	53.5	49.94
Heat Transfer, $\dot{Q}$ (kW)	35.39	35.14	35.34	35.15	34.48
Conversion Efficiency (%)	1.26	1.23	1.13	1.26	1.25

[a] Maximum net power performance is under the condition of $T_{c,in} = 20$ °C (pure water) and $T_{h,in} = 90$ °C (saturated NaCl), with the design constrain $w_c = w_h$ and $\dot{V}_c = \dot{V}_h$.

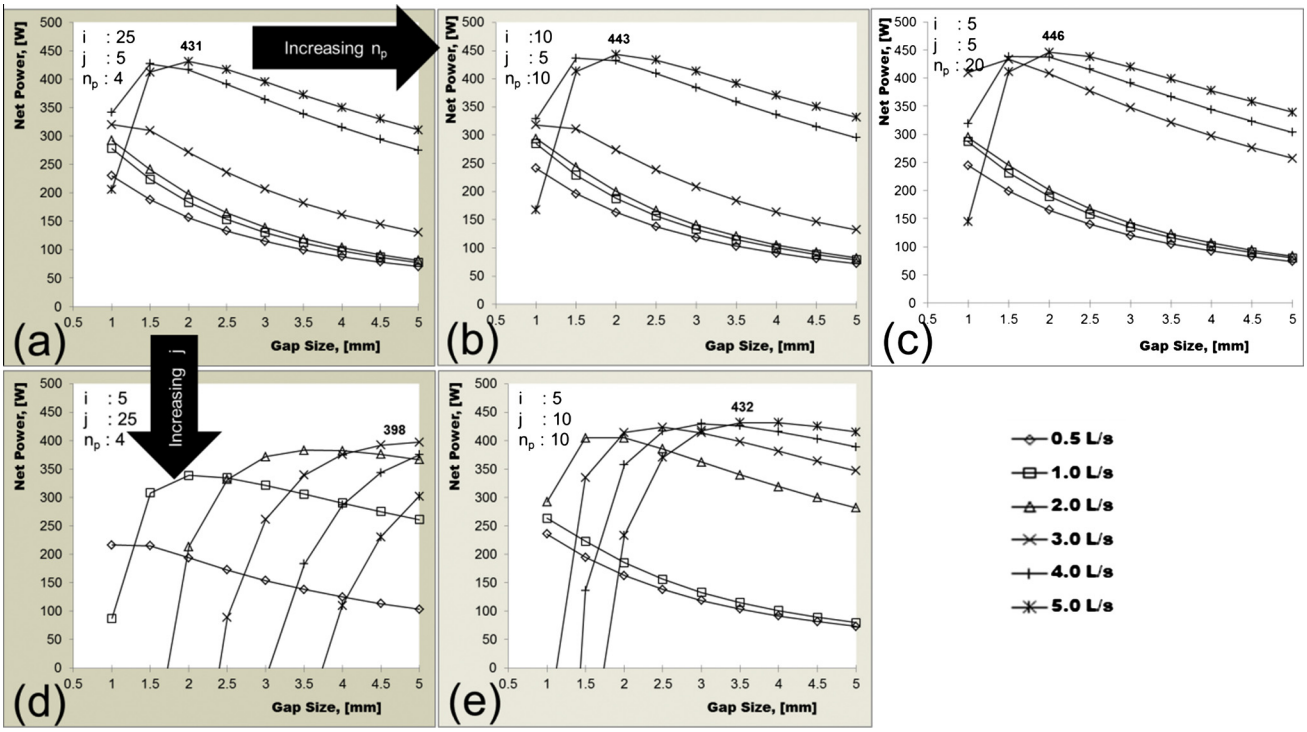

Fig. 9. The theoretical performance of PTPGU with 500 TECs.

configurations of arranging these 500 TECs are proposed, as shown in Table 4. Fig. 9 illustrates the theoretical performance of the proposed PTPGU configurations against the variation in the flow rate and gap size. The theoretical maximum net power produced by each proposed configuration is summarised in Table 4. In light of the result presented in Table 4, the $i \times j \times n_p$ of $5 \times 5 \times 20$ was selected for the fabrication of test rig since it possesses highest maximum net power as well as highest conversion efficiency.

4. Fabrication and experimental testing

4.1. The fabrication

Up to this point, no consideration has been rendered on how the series and parallel connections will impact the performance of electric power generated from the heat exchanger. During the process of heat-electric conversion, the TEC experience ohmic losses due to Joule effect. The TECs' performance from serial and parallel connection are tested and studied by Montecucco et al. [28]. Under temperature mismatch condition (the condition where the TECs connected expose to unequal hot side temperature), series connection performs better than parallel connection. Parallel connection resulted in higher current flow (lower voltage) and hence higher ohmic losses (I^2r). However, TECs connection in series has a potential disadvantage. Single failed TEC connected in series will result in a failed connection in series. In order to avoid such unresponsive system, bypass diodes are needed and this will incur extra cost on the design. In order to minimise the connection of a failed TEC into the system, the connectivity of the TECs were check prior attaching to the stainless steel plate by using Artic Silver® Thermal Adhesive. Fig. 10 shows the wiring diagram of PTPGU. The internal resistance, r of the TEC used ranges from 1.2 to 1.9 Ω with an average value of 1.6 Ω. Hence, the total electrical resistance for the circuit shown in Fig. 10 is equivalent to $20r$, at an average of 32 Ω.

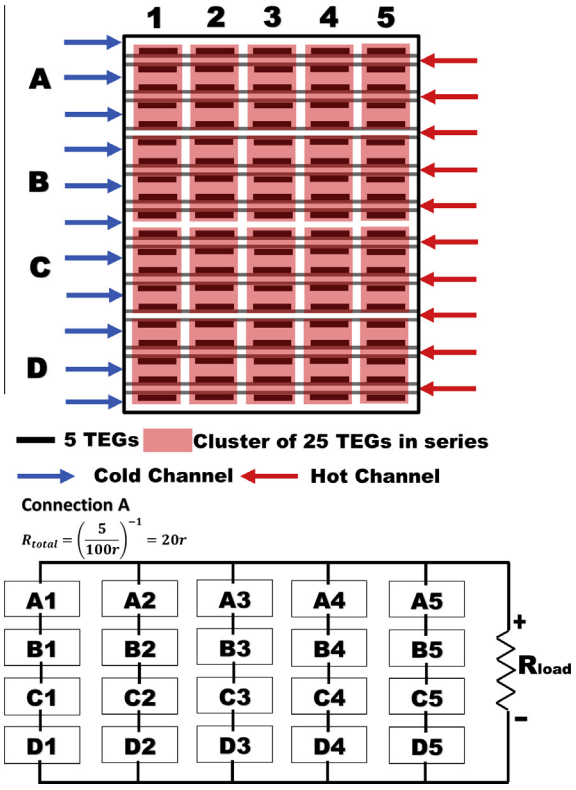

Fig. 10. Wiring diagram for the PTPGU.

The TECs were attached to the stainless steel (304) plates at the hot side of TECs by using Artic Silver® Thermal Adhesive and slotted into acrylic blocks where the water inlets and water outlets located. All of the TECs were exposed to the cold channel. The gap size of the hot and cold channels between the each plate after the assembly is equal to 4 mm and 4.5 mm, respectively. The unit constructed has an overall dimension of 410 mm (L) × 284 mm (W) × 345 mm (H). The wires from the plates are extended out and connected by a wire connections box according to the wiring diagram in Fig. 10 before connecting to the electrical load. In order to avoid the leakage and mixing of water between cold and hot streams, the gap between the plates slotted in the acrylic is sealed with grease and heavy duty PTFE seal tape. The leakage and mixing were tested by introducing only cold water into the PTPGU and no water in the hot channels in order to create maximum head for the leakage of cold water to the adjacent hot channels. Under this condition, the leakage is less than 5% of the cold water introduced. Again, under operating condition where the there is no head difference between cold and hot channels (i.e. both hot and cold channels were filled with water), there is no mixing of both hot and cold streams as the value of α and β were found to be zero in Eqs. (14) and (15).

$$\dot{V}_{c,out} = \dot{V}_{c,in} + \alpha(\dot{V}_{h,in} - \dot{V}_{c,in})$$

$$\alpha = \frac{\dot{V}_{c,out} - \dot{V}_{c,in}}{\dot{V}_{h,in} - \dot{V}_{c,in}} \tag{14}$$

$$\dot{V}_{h,out} = \dot{V}_{h,in} + \beta(\dot{V}_{c,in} - \dot{V}_{h,in})$$

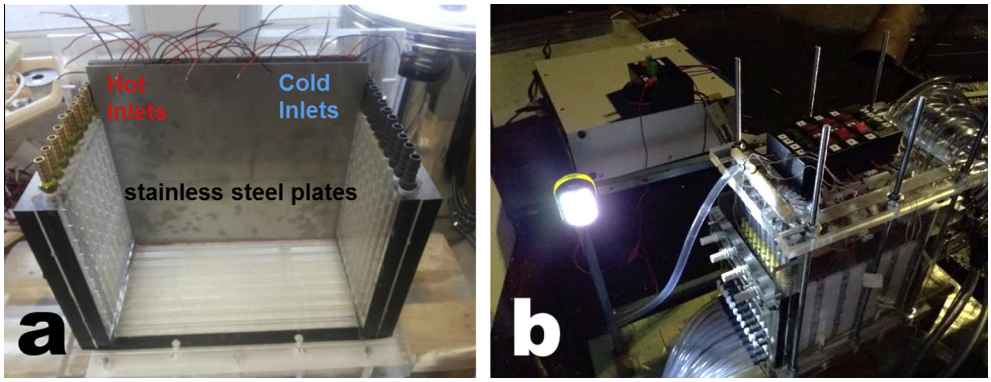

Fig. 11. The PTPGU under construction (a) and under operation (b).

$$\beta = \frac{\dot{V}_{h,out} - \dot{V}_{h,in}}{\dot{V}_{c,in} - \dot{V}_{h,in}} \quad (15)$$

The inner view of the PTPGU is shown in Fig. 11(a) where the stainless steel plates are slotted into the groove created with acrylic and the completed PTPGU under operation by extracting the heat from RMIT SP is shown in Fig. 11(b).

Prior to the experimental testing of PTPGU, the flow distribution of the unit was visualised using a dye at both high and low boundaries of the flow rate that will be tested in the experiment. From Fig. 12, it shows that the distribution of water is considerably uniform throughout the top and bottom of the plate.

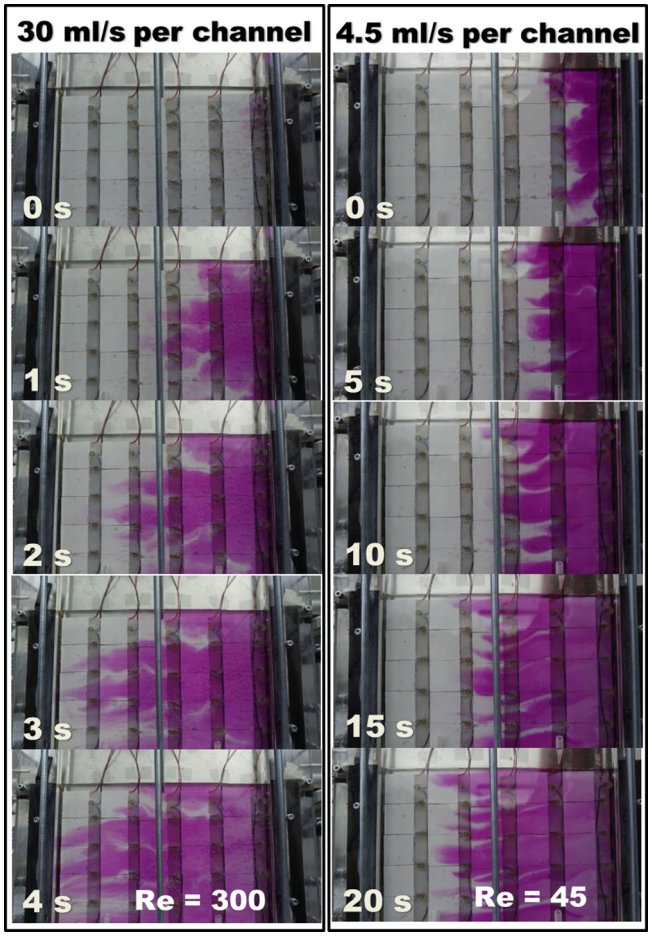

Fig. 12. Flow visualisation of the PTPGU at 30 ml/s (Re = 300) and 4.5 ml/s (Re = 45) per channel.

4.2. The testing

The first part of the testing of the PTPGU was conducted at outdoor by connecting the hot inlet of the unit to the heat extraction piping of the RMIT SP. Meanwhile, for the cold water supply, instead of using the cold water from UCZ, the cold inlet of the unit is connected to the cold water supply from the main since the water temperature of UCZ and cold water supply is in the vicinity of daily average ambient temperature. Since the hot water was supplied through the heat extracted from the 50 m^2 SP at RMIT, hence there is no control for the hot side temperature. As the heat extraction continues, the heat stored in the solar pond reduces and consequently the temperature of the hot water temperature drops. As a result, the PTPGU was operating in a pseudo-steady state. The data presented is the result of averaging the reading for 2 min. Therefore, the hot side temperature reading was taken in 'as it' condition rather than controlling the hot side temperature, similar to the actual condition if this system operate on-site. The inlet and outlet temperature for both cold and hot streams were measured using type T thermocouples of ±1 °C accuracy with Agilent data logger 34870A, connected and recorded through a computer. On the other hand, the water flow rate of cold and hot streams were measured using domestic water flow meters throughout the experiment. The electrical resistance of the load was supplied through Kikusui Electronic Load PLZ1004W and subsequently, the voltage and current were measured using this unit at accuracies of 0.1% and 0.2%, respectively.

Figs. 13 and 14 present the performance of PTPGU at varying load resistance, which are skewed at high resistance. Maximum power output was generated at resistance of $R_L = 32\ \Omega$. The power output increase significantly from short circuit condition to matching load condition and gradually decreases after exceeding the internal electrical resistance of the PTPGU. On the other hand, Figs. 15 and 16 show the performance curve of PTPGU subjected

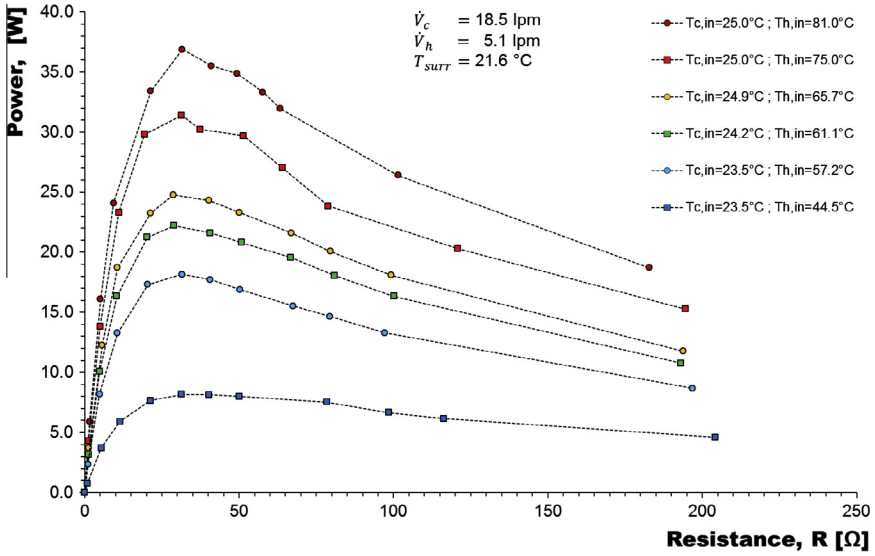

Fig. 13. Performance of the PTPGU at $\dot{V}_c = 18.5$ lpm; $\dot{V}_h = 5.1$ lpm under varying load resistance.

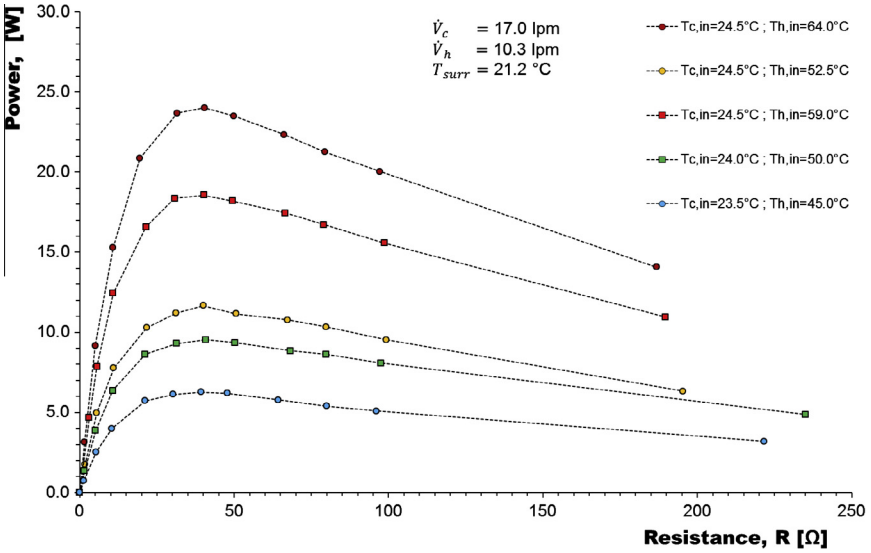

Fig. 14. Performance of the PTPGU at $\dot{V}_c = 17.0$ lpm; $\dot{V}_h = 10.3$ lpm under varying load resistance.

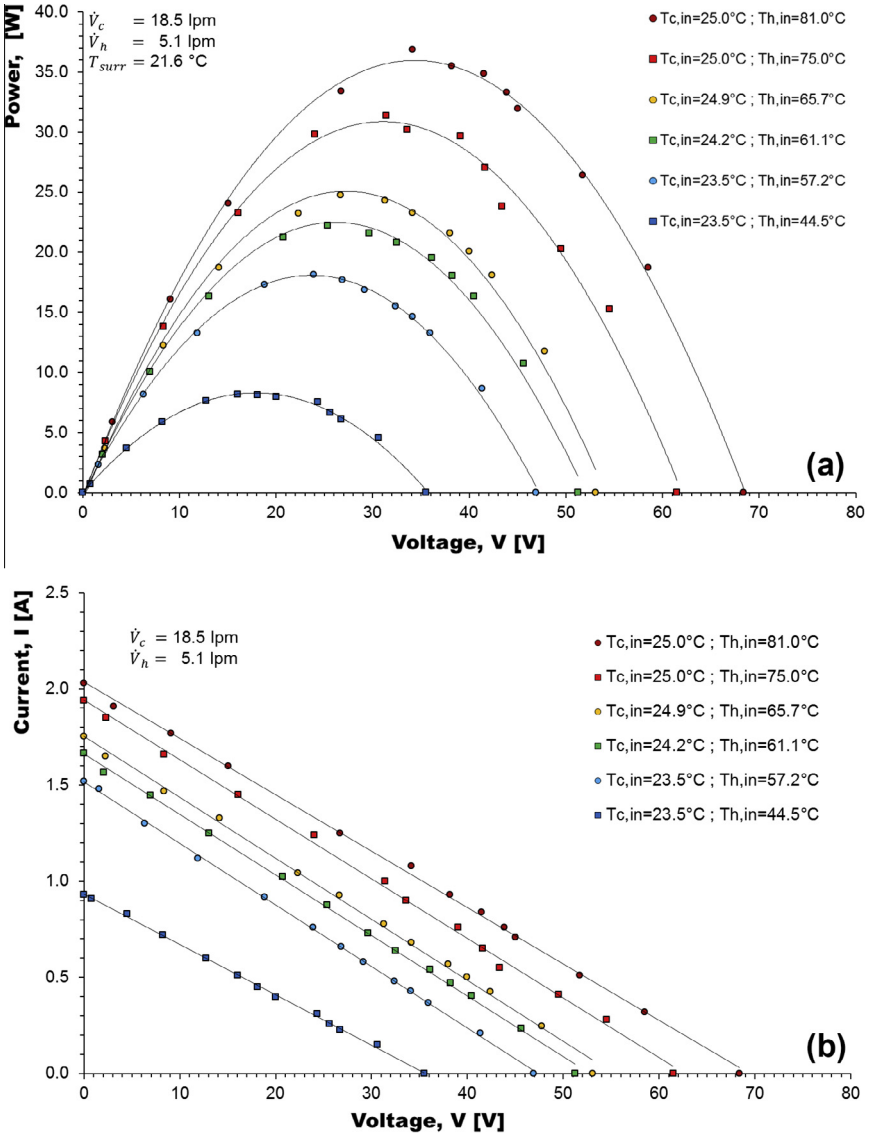

Fig. 15. Performance of the PTPGU at $\dot{V}_c = 18.5$ lpm; $\dot{V}_h = 5.1$ lpm (a) Power-Voltage and (b) Curent-Voltage.

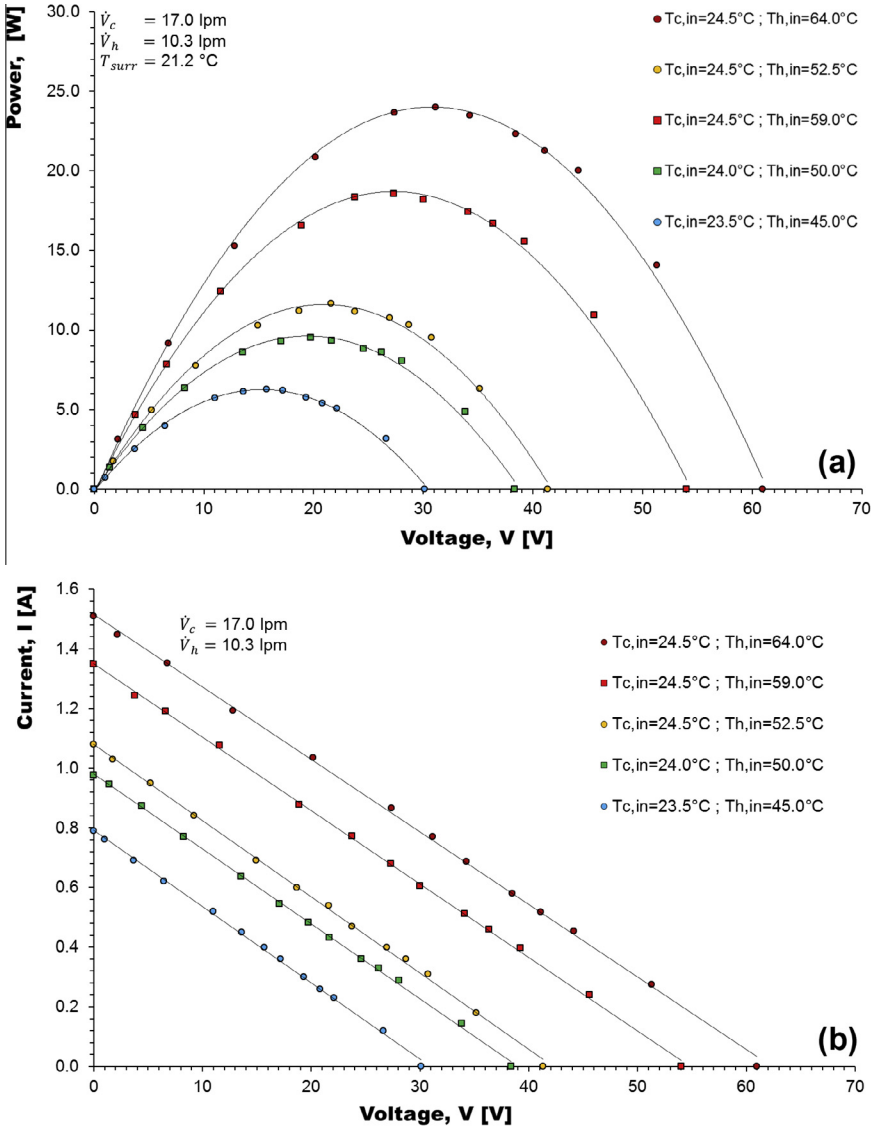

Fig. 16. Performance of the PTPGU at $\dot{V}_c = 17.0$ lpm; $\dot{V}_h = 10.3$ lpm (a) Power-Voltage and (b) Current-Voltage.

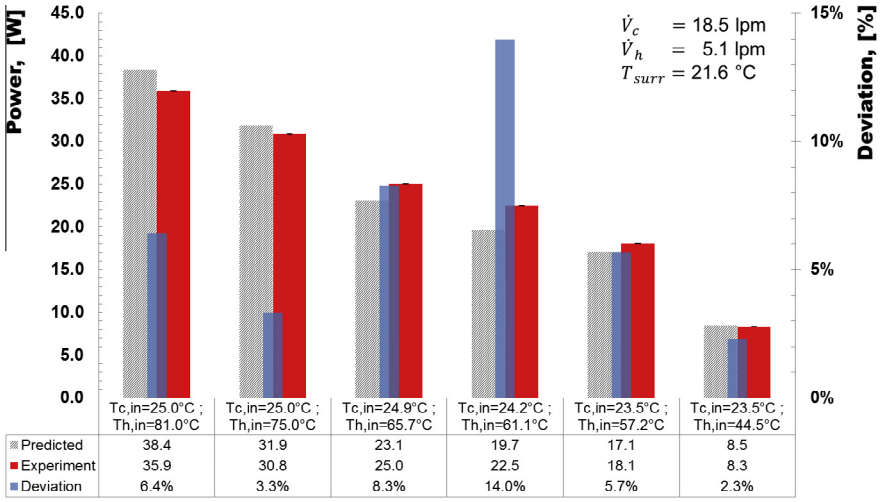

Fig. 17. Theoretical and experimental comparison of PTPGU at $\dot{V}_c = 18.5$ lpm; $\dot{V}_h = 5.1$ lpm.

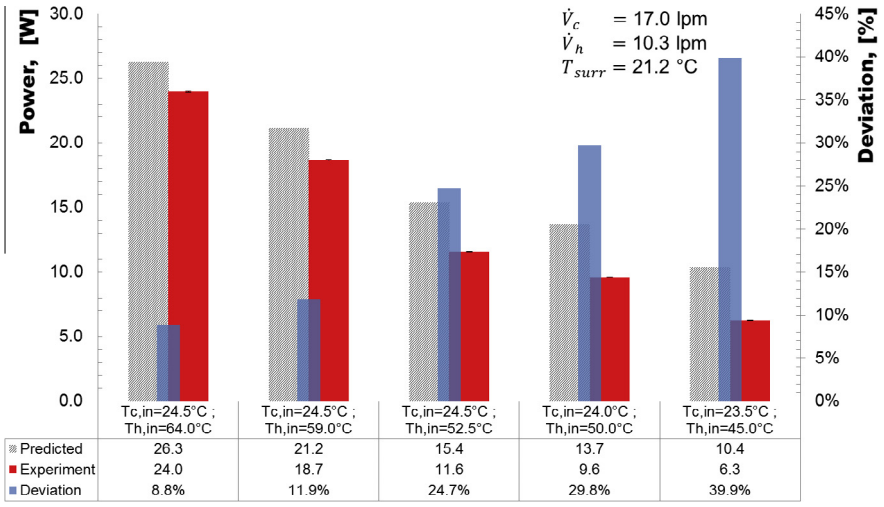

Fig. 18. Theoretical and experimental comparison of PTPGU at $\dot{V}_c = 17.0$ lpm; $\dot{V}_h = 10.3$ lpm.

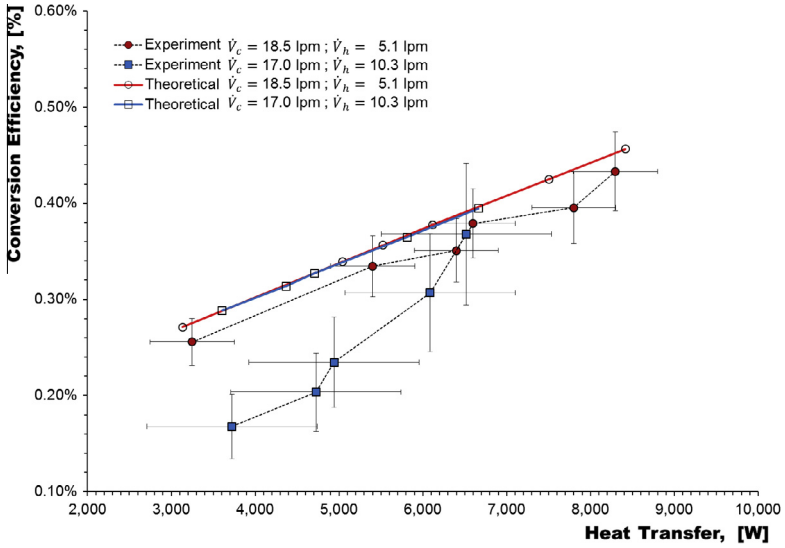

Fig. 19. A comparison of experimental and theoretical conversion efficiency against heat transfer for the ΔT tested in this study.

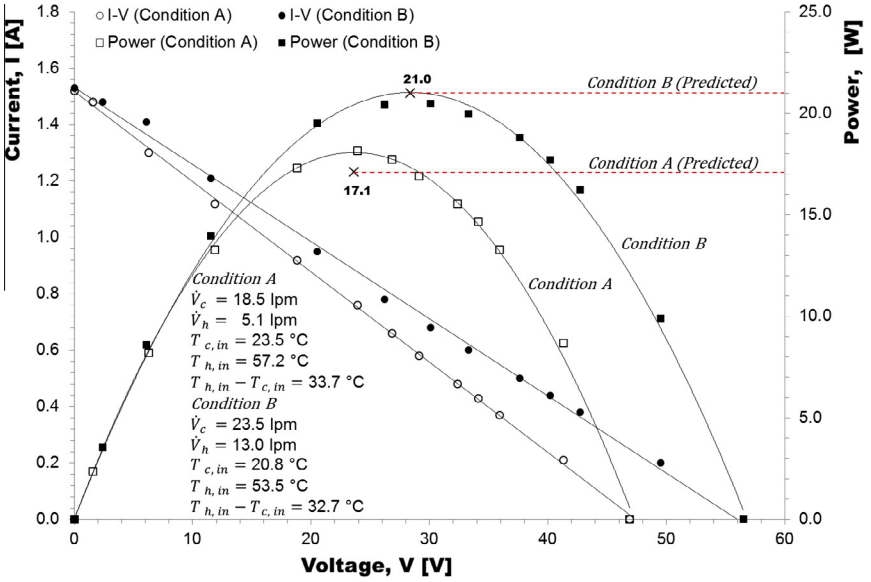

Fig. 20. The effect of flow rate on the power output of PTPGU.

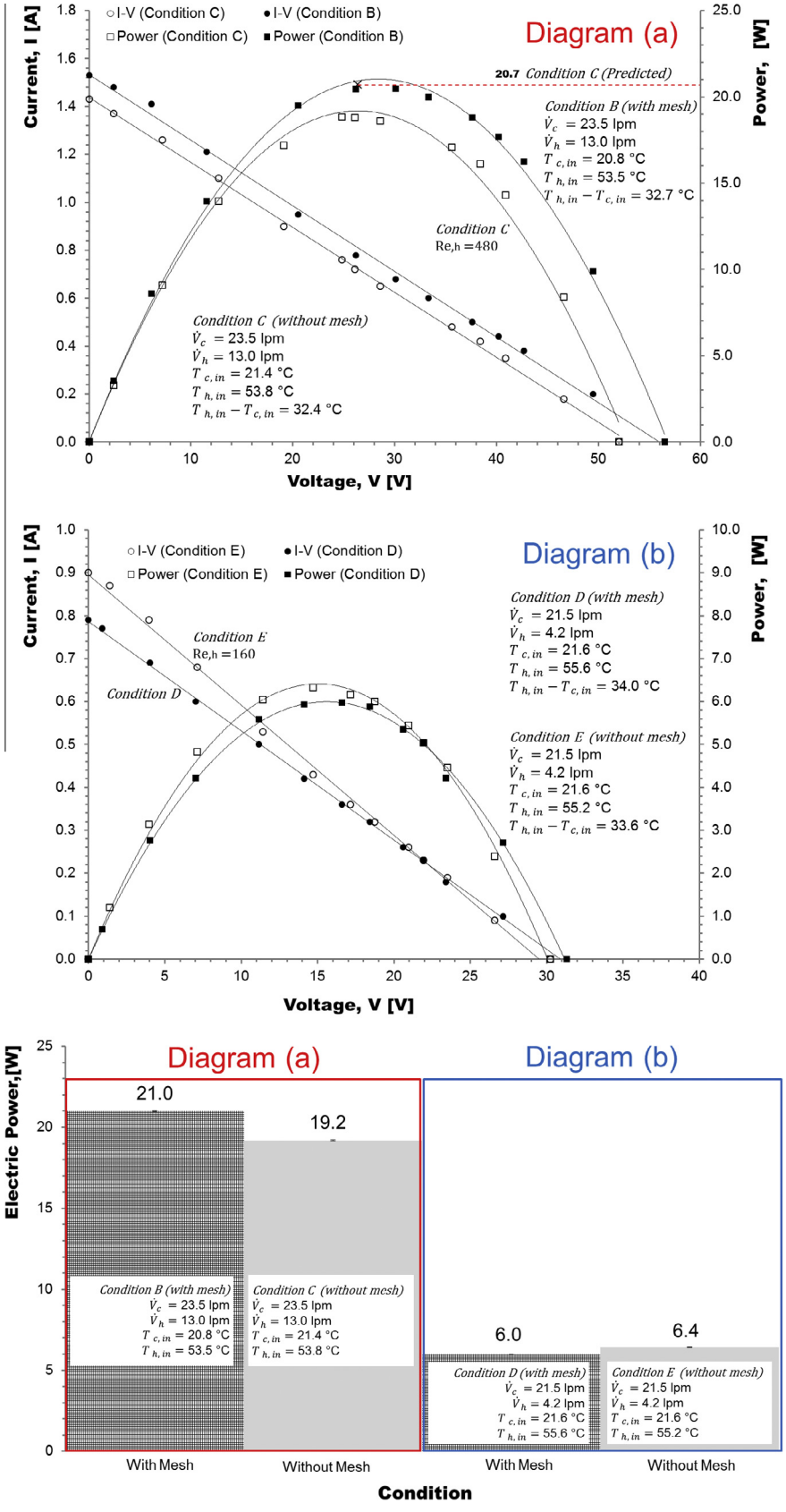

Fig. 21. The effect of copper mesh insertion on the power output of PTPGU.

to varying water temperature of hot water inlet at different hot water flow rate. The flow rate at the cold side was supplied at the flow rate of domestic water supply which usually has a range from 17 to 24 LPM. Clearly, under this flow rate, the flow in the PTPGU is in the laminar flow regime whereby the flow observation shown in Fig. 12 advocates the evident. Under the SP heat extraction mode, usually the flow rate in the heat exchanger piping is vicinity of 0.2 L/s (12 LPM), which is achievable even if the system utilised the water supply from the main for the heat extraction from LCZ. The implication of using the water supply from the main is the elimination of the use of pump. Thus, the electrical power obtained from the experiment, $\dot{W}_{max}$ corresponds to the net power. The hot side temperature for the experiment conducted was in the range of 40–80 °C which corresponds to normal operating temperature of the LCZ under heat extraction mode. With the hot side flow rate of 5.1 LPM at 81 °C, the unit generates 35.9 W. The maximum power point in the P-V curve is corresponding to $\frac{1}{4}I_{sc}V_{oc}$ in the I-V curve. Higher ΔT will produce higher maximum power as $\dot{W}_{max} \propto \Delta T^2$. At $\dot{V}_c = 17.0$ LPM and $\dot{V}_h = 10.3$ LPM (Fig. 16), the highest $T_{h,in}$ tested is 64 °C. This is corresponding to the annual average LCZ temperature of a typical operating solar pond heat extraction efficiency of 10%. The power generation is relatively sensitive to ΔT compared to the change in flow rate in laminar flow regime. Reducing the inlet temperature difference, $(T_{h,in} - T_{c,in})$ by 5 °C resulted in 22% drop in the power produced and 11 °C reduction of inlet temperature caused the power produced decreased by 52% from 35.9 W. On the other hand, Figs. 17 and 18 depict the deviation of the experimental results with the predicted PTPGU performance using the theoretical model proposed in the earlier section. The deviations shown in Fig. 17 ranged from 2.3 to 14%. Hence, the theoretical model proposed is adequate to predict the performance of PTPGU for the flow rate stipulated. In Fig. 18, the deviations between experimental and theoretical results spaned from 8.8 to 39.9%. Relatively higher errors are found for lower inlet temperature difference when lower electric power to be produced is expected.

The conversion efficiency of the PTPGU, η_t is defined as $\eta_t = \frac{\dot{W}_{max}}{\dot{Q}}$. As defined, the experimental uncertainty, $\omega_U = \left[\left(\frac{\partial U}{\partial x_1}\omega_1\right)^2 + \left(\frac{\partial U}{\partial x_2}\omega_2\right)^2 + \cdots + \left(\frac{\partial U}{\partial x_n}\omega_n\right)^2\right]^{0.5}$ where U is a function of independent variable of $x_1, x_2, \ldots, x_n$. In this study, for the measurement of heat transfer, as $\dot{Q} = \rho\dot{V}C_p\Delta T$, hence $\omega_{\dot{Q}} = \dot{Q}\left[\left(\frac{\omega_{\dot{V}}}{\dot{V}}\right)^2 + \left(\frac{\omega_{\Delta T}}{\Delta T}\right)^2\right]^{0.5}$. Meanwhile, for $\dot{W} = I \times V$, $\omega_{\dot{W}} = \dot{W}\left[\left(\frac{\omega_I}{I}\right)^2 + \left(\frac{\omega_V}{V}\right)^2\right]^{0.5}$. Finally, as $\eta_t = \frac{\dot{W}_{max}}{\dot{Q}}$, $\omega_{\eta_t} = \eta_t\left[\left(\frac{\omega_{\dot{W}_{max}}}{\dot{W}_{max}}\right)^2 + \left(\frac{\omega_{\dot{Q}}}{\dot{Q}}\right)^2\right]^{0.5}$. The result for conversion efficiencies of the PTPGU tested is presented in Fig. 19, with maximum conversion efficiency, η_t of 0.43%. The Carnot efficiency at this condition is 15.8%. By considering the thermal-electrical conversion efficiency of the commercially available TEC is about 8–10% of the Carnot efficiency, ideally the system could achieve a peak of 1.26–1.58% conversion efficiency at a sufficiently high flow rate when the convective thermal resistant is low. The flow rates tested in this work are within the regime of laminar flow (by using the supply from the main without the use of pump), hence there will be no significant different or improvement due to the flow increment, as shown in Fig. 19.

In the second part of the testings, the PTPGU was tested at indoor. It is evident from Fig. 20 that, as we increase the flow rate of PTPGU (from condition A to condition B), the $\dot{W}_{max}$ produced increased from 18.1 W to 21.0 W (i.e. output increase of 16%). Hence, the electric output produced is insensitive to the increment in flow rate since changing from condition A to condition B, the flow rate, $\dot{V}_h$ increases by 250%.

The effect of mesh insert to enhance the heat transfer had been studied and presented by Dewan et al. [29]. In the later stage of the testing, two layers of copper mesh of mesh number of 10 with 0.4 mm diameter had been introduced into the hot channel in order to enhance the heat transfer. Fig. 21 demonstrates the effect of copper mesh insertion into the hot channels of PTPGU and being

Table 5
The effect of copper mesh insertion on the heat transfer of PTPGU.

Flow rate	Mesh	Temperature (°C)	Heat transfer (W)	Uncertainty (W)
$\dot{V}_c = 23.5$LPM; $\dot{V}_h = 13.0$ LPM	With mesh (Condition B)	$T_c = 20.8$; $T_h = 53.5$	8135	±2118
	Without mesh (Condition C)	$T_c = 21.4$; $T_h = 53.8$	7693	±2118
$\dot{V}_c = 21.5$ LPM; $\dot{V}_h = 4.2$ LPM	With mesh (Condition D)	$T_c = 21.6$; $T_h = 55.6$	5457	±414
	Without mesh (Condition E)	$T_c = 21.4$; $T_h = 55.2$	4363	±414

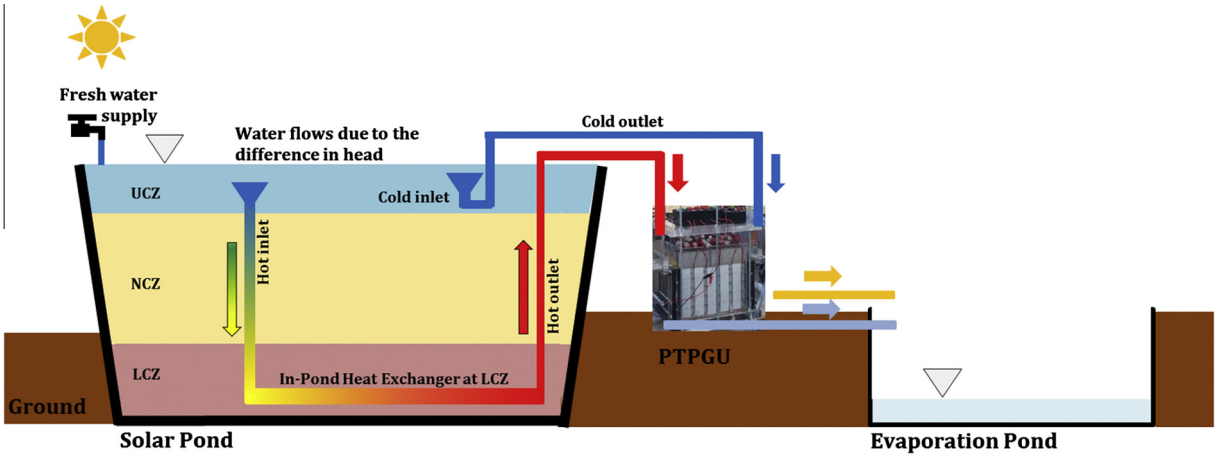

Fig. 22. Proposed design of SP-PTPGU system with PTPGU without the use of pump.

compared in two distinct $\dot{V}_h$, which are 13.0 LPM and 4.1 LPM. The result shows that there is 9.4% increment in the output power produced for $\dot{V}_h = 13.0$ LPM whereas for $\dot{V}_h = 4.1$ LPM, there is ambiguous conclusion can be drawn since the power produced with and without the mesh are 6.0 W and 6.4 W (a difference of 0.4 W), respectively. The heat transfer enhancement of the copper mesh insertion is presented in Table 5, which corresponds to diagram (a) and diagram (b) of Fig. 21.

In practice, the UCZ of SP needs to be constantly flushed with the fresh water in order to compensate the evaporation loss as well as reducing the salinity at UCZ due to the upward salt diffusion from LCZ. Taking an practical example of the RMIT SP, this SP require a constant fresh water flow about 6×10^{-3} to 1×10^{-2} LPM/m^2 for surface washing. As illustrated in Fig. 3, the water supplied to the PTPGU can be recirculated back to the SP for the regular surface flushing. In contrast to the PTPGU system proposed in Fig. 3, Fig. 22 introduces an alternative SP-PTPGU system. The system proposed in Fig. 22 requires the water to be circulated into PTPGU via the difference in water head. Hence, instead of discharging the excess water through the surface flushing or overflow system, the low salinity fresh water from the UCZ is circulated into LCZ. After gaining the heat from LCZ, the hot water will pass through PTPGU before being collected in the evaporation pond so that upon the evaporation process, the salt content collected can be reused.

5. Conclusion

This paper has presented a proof of concept on the electric power generation by TECs with solar ponds experimentally, operated under different conditions. The PTPGU proposed is subjected to an open channel flow. The study started by addressing the design issues of PTPGU, followed by the theoretical modelling on heat transfer of PTPGU before estimating the electric output using the performance curve of single TEC. The PTPGU fabricated was then tested after ensuring a good flow distribution via visualisation. From the testing conducted, electrical power output of 35.9 W was generated under the condition of $\dot{V}_c = 18.5$ LPM and $\dot{V}_h = 5.1$ LPM at the temperature of $T_{c,in} = 25$ °C and $T_{h,in} = 81$ °C. It has been shown that the theoretical model proposed is adequate to predict the performance of the PTPGU after comparing the performance of the PTPGU obtained experimentally with the theatrical prediction. Furthermore, it has been shown in this work that, small degree in performance enhancement of the PTPGU is possible through copper mesh insertion.

References

[1] Rowe DM. Thermoelectrics, an environmentally-friendly source of electrical power. Renew Energy 1999;16(1):1251–6.
[2] Bell LE. Cooling, heating, generating power, and recovering waste heat with thermoelectric systems. Science 2008;321(5895):1457–61.
[3] Goldsmid HJ. Bismuth telluride and its alloys as materials for thermoelectric generation. Materials 2014;7(4):2577–92.
[4] Zheng XF, Liu CX, Yan YY, Wang Q. A review of thermoelectrics research–recent developments and potentials for sustainable and renewable energy applications. Renew Sust Energy Rev 2014;32:486–503.
[5] He W, Zhang G, Zhang X, Ji J, Li G, Zhao X. Recent development and application of thermoelectric generator and cooler. Appl Energy 2015;143:1–25.
[6] Yu J, Zhao H. A numerical model for thermoelectric generator with the parallel-plate heat exchanger. J Power Sources 2007;172(1):428–34.
[7] Niu X, Yu J, Wang S. Experimental study on low-temperature waste heat thermoelectric generator. J Power Sources 2009;188(2):621–6.
[8] David B, Ramousse J, Luo L. Optimization of thermoelectric heat pumps by operating condition management and heat exchanger design. Energy Convers Manage 2012;60:125–33.
[9] Rodríguez A, Vián JG, Astrain D, Martínez A. Study of thermoelectric systems applied to electric power generation. Energy Convers Manage 2009;50(5):1236–43.
[10] Crane DT, Jackson GS. Optimization of cross flow heat exchangers for thermoelectric waste heat recovery. Energy Convers Manage 2004;45(9):1565–82.
[11] Suter C, Jovanovic ZR, Steinfeld A. A 1kWe thermoelectric stack for geothermal power generation–modeling and geometrical optimization. Appl Energy 2012;99:379–85.
[12] Gou X, Xiao H, Yang S. Modeling, experimental study and optimization on low-temperature waste heat thermoelectric generator system. Appl Energy 2010;87(10):3131–6.
[13] Nnanna AA, Rutherford W, Elomar W, Sankowski B. Assessment of thermoelectric module with nanofluid heat exchanger. Appl Therm Eng 2009;29(2):491–500.
[14] Liu X, Deng YD, Li Z, Su CQ. Performance analysis of a waste heat recovery thermoelectric generation system for automotive application. Energy Convers Manage 2015;90:121–7.
[15] deok In B, ik Kim H, wook Son J, hyung Lee K. The study of a thermoelectric generator with various thermal conditions of exhaust gas from a diesel engine. Int J Heat Mass Transfer 2015;86:667–80.
[16] Lu H, Wu T, Bai S, Xu K, Huang Y, Gao W, Yin X, Chen L. Experiment on thermal uniformity and pressure drop of exhaust heat exchanger for automotive thermoelectric generator. Energy 2013;54:372–7.
[17] Wang Y, Li S, Yang X, Deng Y, Su C. Numerical and experimental investigation for heat transfer enhancement by dimpled surface heat exchanger in thermoelectric generator. J Electron Mater 2016;45(3):1792–802.
[18] Wang T, Luan W, Liu T, Tu ST, Yan J. Performance enhancement of thermoelectric waste heat recovery system by using metal foam inserts. Energy Convers Manage 2016;124:13–9.
[19] He W, Wang S, Zhao Y, Li Y. Effects of heat transfer characteristics between fluid channels and thermoelectric modules on optimal thermoelectric performance. Energy Convers Manage 2016;113:201–8.
[20] Hsu CT, Huang GY, Chu HS, Yu B, Yao DJ. Experiments and simulations on low-temperature waste heat harvesting system by thermoelectric power generators. Appl Energy 2011;88(4):1291–7.
[21] Sasaki K, Horikawa D, Goto K. Consideration of thermoelectric power generation by using hot spring thermal energy or industrial waste heat. J Electron Mater 2015;44(1):391–8.
[22] Massaguer E, Massaguer A, Montoro L, Gonzalez JR. Modeling analysis of longitudinal thermoelectric energy harvester in low temperature waste heat recovery applications. Appl Energy 2015;140:184–95.
[23] Bjørk R, Sarhadi A, Pryds N, Lindeburg N, Viereck P. A thermoelectric power generating heat exchanger: Part I-Experimental realization. Energy Convers Manage 2016;119:473–80.
[24] Tchanche BF, Lambrinos G, Frangoudakis A, Papadakis G. Low-grade heat conversion into power using organic Rankine cycles–a review of various applications. Renew Sust Energy Rev 2011;15(8):3963–79.
[25] Singh B, Remeli MF, Chet DL, Oberoi A, Date A, Akbarzadeh A. Experimental investigation on effect of adhesives on thermoelectric generator performance. J Electron Mater 2015;44(6):1864–9.
[26] Wang YF, Akbarzadeh A. A study on the transient behaviour of solar ponds. Energy 1982;7(12):1005–17.
[27] Sharqawy MH, Lienhard JH, Zubair SM. Thermophysical properties of seawater: a review of existing correlations and data. Desalin Water Treat 2010;16(1–3):354–80.
[28] Montecucco A, Siviter J, Knox AR. The effect of temperature mismatch on thermoelectric generators electrically connected in series and parallel. Appl Energy 2014;123:47–54.
[29] Dewan A, Mahanta P, Raju KS, Kumar PS. Review of passive heat transfer augmentation techniques. P I Mech Eng A-J Pow 2004;218(7):509–27.